

Location Optimization and Resource Allocation of IRS in a Multi-User Indoor mmWave VR Network

Jalal Jalali*, Maria Bustamante Madrid*, Filip Lemic[†], Hina Tabassum[‡],

Jakob Struye*, Jeroen Famaey*, Xavier Costa Perez^{†§}

*Internet and Data Lab, University of Antwerp - imec, Belgium

[†]AI-Driven Systems Lab, i2Cat Foundation, Spain

[‡]Electrical Engineering and Computer Science Department, York University, Canada

[§]NEC Labs Europe GmbH, Germany and ICREA, Spain

Email: filip.lemic@i2cat.net

Abstract—Next-generation Virtual Reality (VR) technology enables full-user immersion and support for multiuser Virtual Experiences (VEs). Given the low-cost and passive nature of intelligent reflecting surfaces (IRSs), this paper investigates the optimal design of a multi-user IRS-assisted VR network, where an IRS is optimally deployed in a confined space as a function of VR fully-immersed users' trajectory. In particular, we consider sum-rate maximization of all VR users and optimize the Access Point's (AP) active beamforming, and the IRS's placement, phase shifts, and radiation patterns in a confined indoor environment operating in millimeter Wave (mmWave) frequencies. We introduce the Alternating Optimization (AO) algorithm, decompose the problem into distinct sub-problems, and solve each problem optimally. That is, maximum-ratio transmission (MRT) is applied for optimal beamforming at the AP, optimal closed-form IRS phase shifts are determined using quadratic transformation, global optimization is conducted to determine the ideal locations for the IRS elements, and the monotonic optimal radiation pattern has been analyzed. Our findings highlight that strategically allocating the IRS's resources at optimal physical locations enhances signal stability and maximizes per-user throughput.

Index Terms—Alternative Optimization (AO), Intelligent Reflecting Surface (IRS), Resource Allocation, Millimeter Wave (mmWave), Virtual Reality (VR).

I. INTRODUCTION

VIRTUAL REALITY (VR) is anticipated to transform our digital interactions in various domains such as healthcare, tourism, education, entertainment, and occupational safety [1]. VR systems are poised to accommodate multiple fully-immersed users who can freely navigate their Virtual Experiences (VEs) in an indoor environment. To enable cost-effective indoor VEs, the deployment of Intelligent Reflective Surfaces (IRSs) on the walls as a function of users' trajectory is a potential solution [2]. An IRS consists of large arrays of passive reflecting elements on a reconfigurable planar surface. These elements can independently modify the phase of an incoming signal before reflecting it towards its intended receiver. The IRS can be a boon for users experiencing

This study was supported by MCIN/AEI/10.13039/01100-011033/ FEDER/EU HoloMit 2.0 (PID2021-126551OB-C21), and the Recovery Plan's UNICO I+D 5G (nr. TSI-063000-2021-7-Open6G: Smart Surfaces for Joint Communications and Sensing Systems), sponsored by the Spanish Ministry of Economic Affairs and NextGeneration EU. Additionally, the CHIST-ERA grant SAMBAS (CHIST-ERA-20-SICT-003) backed this work through FWO, ANR, NKFH, and UKRI. This research was partly funded by the FWO WaveVR project (grant number: G034322N)

significant path loss or blockage on the direct link, especially when primarily operating in the millimeter Wave (mmWave) frequency band, as the IRS creates additional propagation pathways — namely, reflected channels [3]. Moreover, the IRS offers added degrees of freedom through the phase shifts of the reflective elements, which can be harnessed to minimize interference [4]. It is also worth noting that IRSs are envisioned to be manufactured as passive, cheap, and flexible entities adaptable for indoor VR streaming setups, as they could be used as “soft” environmental boundaries [5].

Prior research has underscored the advantages of integrating IRSs into traditional multi-user wireless communication frameworks [4], [6]–[8]. For instance, Chaccour *et al.* demonstrated that the IRS can enhance both the sum data-rate and the reliability of data transfer in VR contexts [6]. Jalali *et al.* delved into the IRS design for energy efficiency and admission control maximization for Internet of Things (IoT) users with short packet lengths [4]. Besser *et al.* introduced a phase hopping algorithm tailored for IRS-supported systems to elevate data transfer reliability without the necessity for channel state information (CSI) [7]. Furthermore, Zhou *et al.* studied a latency minimization problem for a multi-user secure IRS-aided VR delivery network with imperfect CSI [8].

To the best of our knowledge, none of the research works have optimized the design of an IRS-assisted indoor VR network, where the IRS is considered to be deployed in a confined 3-Dimensional (3D) space as a function of VR users' trajectory.

In this paper, we consider an IRS-enabled multi-user mmWave VR environment (see Figure 1), where the IRS is deployed on one of the walls, and a multi-antenna AP transmits data to a set of single-antenna Head Mounted Devices (HMDs) via the IRS. Specifically, we maximize the aggregate data rate of all HMDs by optimizing the location of the IRS, beamforming, phase shifts, and radiation patterns as a function of VR users' trajectory (modeled using redirected walking) in a confined indoor environment. The formulated problem is non-convex, thus we employ Alternating Optimization (AO) algorithm, segmenting the main optimization problem into four distinct sub-problems, in which each sub-problem is optimally solved. For the first sub-problem, i.e., the active beamforming at the AP, the maximum-ratio transmission (MRT) is proved to be the optimal AP beamformer. In the second sub-problem,

Real-time-operating IRS for optimizing the communication coverage homogeneity

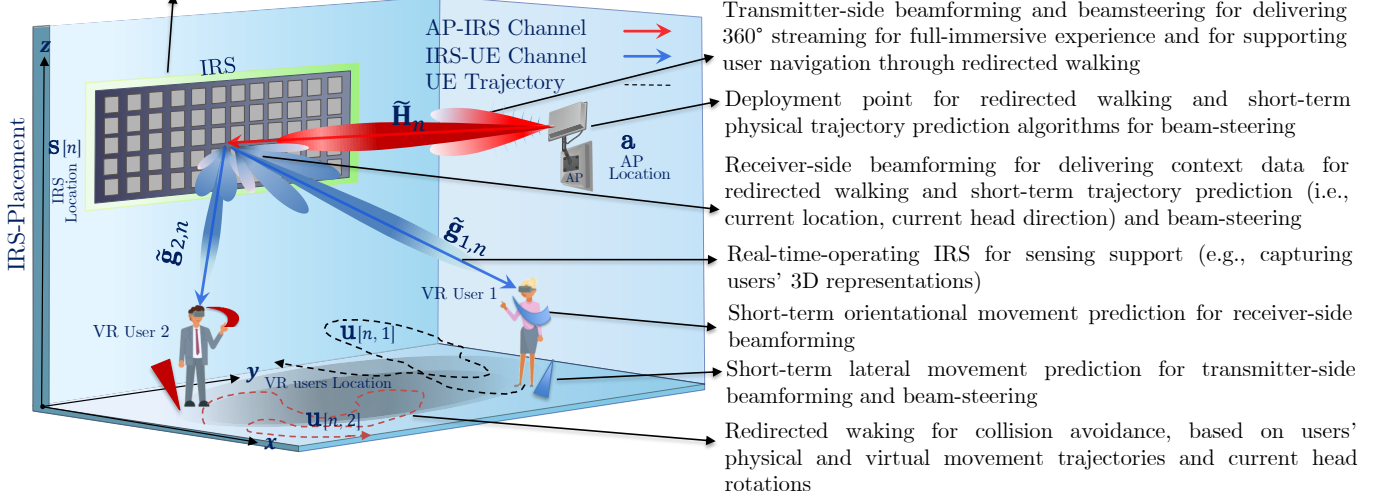


Fig. 1: Considered multi-user IRS-assisted full-immersive Virtual Reality scenario.

a closed-form optimal solution is obtained for the IRS phase shifts design using quadratic transformation. A global optimization of the IRS's placement is carried out in the third sub-problem based on a first-order derivative of the objective function. Finally, the optimal radiation pattern is determined in a closed-form format based on the monotonicity of the transformed objective function. The simulation results indicate that IRS with passive beamforming and location-based IRS placement, combined with an optimal beamforming at the Access Point (AP), can achieve improved data-rates compared to a number of baseline schemes.

Notations: Boldface lower-case and upper-case letters represent vectors and matrices, respectively, e.g., \mathbf{x} for vectors and \mathbf{X} for matrices. The operators $(\cdot)^T$ and $(\cdot)^H$ are the transpose and the conjugate transpose of a matrix or vector, respectively, while $(\cdot)^*$ gives the optimal value of a matrix or vector. The functions $\text{tr}(\cdot)$, $\text{vec}(\cdot)$, and $\text{diag}(\cdot)$ refer to the trace, vectorization, and diagonalization of a matrix, respectively. The symbol j is defined as $\sqrt{-1}$. Finally, $\Re(\cdot)$ and $\arg(\cdot)$ denote the real and the phase of a complex function, respectively.

II. SYSTEM MODEL AND PROBLEM FORMULATION

As depicted in Figure 1, we consider an IRS-assisted Multi-Input Single-Output (MISO) communication system in which IRSs relays data to a single antenna HMD VR user. The direct link between the transmitter and receiver is considered to be blocked. Doppler effect caused by the HMD's mobility is presumed to be fully compensated. In this network, an AP with L antennas serves a set of HMDs represented as $\mathcal{K} = \{1, \dots, K\}$ using an IRS whose elements are denoted by $\mathcal{M} = \{1, \dots, M\}$. Our goal is to fine-tune the IRS's resource allocation based on a placement optimization problem to achieve maximum Signal-to-Noise Ratio (SNR) over a fixed time span $T > 0$. The time duration T is partitioned

- Transmitter-side beamforming and beamsteering for delivering 360° streaming for full-immersive experience and for supporting user navigation through redirected walking
- Deployment point for redirected walking and short-term physical trajectory prediction algorithms for beam-steering
- Receiver-side beamforming for delivering context data for redirected walking and short-term trajectory prediction (i.e., current location, current head direction) and beam-steering
- Real-time-operating IRS for sensing support (e.g., capturing users' 3D representations)
- Short-term orientational movement prediction for receiver-side beamforming
- Short-term lateral movement prediction for transmitter-side beamforming and beam-steering
- Redirected walking for collision avoidance, based on users' physical and virtual movement trajectories and current head rotations

into N uniformly spaced time intervals, given by $T = N\xi_t$. Specifically, ξ_t denotes the length of each individual time slot, and \mathcal{N} is defined as the set of all these time slots, represented by $\mathcal{N} = \{1, \dots, N\}$.

We adopt a 3D Cartesian coordinate system with the AP at a fixed location $\mathbf{a} = [a_x, a_y, a_z]^T \in \mathbb{R}^{3 \times 1}$. The HMDs are traversing in a fixed ground location, and their trajectory follows the path $\mathbf{u}[n, k] = [u_x[n, k], u_y[n, k], u_z[n, k]]^T \in \mathbb{R}^{3 \times 1}$ based on redirected walking [9]. The location-based allocation of IRS resources, when projected onto the vertical plane, is represented by $\mathbf{s}[n] = [s_x[n], s_y[n], s_z[n]]^T \in \mathbb{R}^{3 \times 1}$. Furthermore, we confine the area of interest to four vertical Cartesian planes \mathcal{H}_1 to \mathcal{H}_4 where the IRS resources could potentially be allocated, with \mathcal{H}_1 being:

$$y_{\min} < s_y[n] < y_{\max}, \quad z_{\min} < s_z[n] < z_{\max}, \\ s_x[n] = \{x_{\min}, x_{\max}\}, \quad \forall n \in \mathcal{N}, \quad (1)$$

$$x_{\min} < s_x[n] < x_{\max}, \quad z_{\min} < s_z[n] < z_{\max}, \\ s_y[n] = \{y_{\min}, y_{\max}\}, \quad \forall n \in \mathcal{N}, \quad (2)$$

and \mathcal{H}_2 to \mathcal{H}_4 could be defined similarly. These regions ensure that the IRS is positioned in one of the corner walls of a room-shaped environment, as seen in Figure 1. We also take into account the radiation pattern of the IRS:

$$F(\psi_k, \varphi) = \begin{cases} \cos^3(\psi_k), & \psi_k \in [0, \pi/2], \varphi \in [0, 2\pi], \\ 0, & \psi_k \in (\pi/2, \pi], \varphi \in [0, 2\pi], \end{cases} \quad (3)$$

where $\psi_k, \forall k \in \mathcal{K} \cup \{0\}$, and φ represent the elevation and azimuth angles, respectively, from the IRS to the AP/HMD link [10]. It is worth pointing out that the radiation pattern of the IRS remains consistent across various azimuth angles. To streamline our discussion, we exclude the argument φ from the function $F(\psi_k, \varphi)$ in (3) in subsequent equations, using $F(\psi_k)$ in place of $F(\psi_k, \varphi)$. Given these conditions, the dynamic

channel between AP and IRS, and between IRS and the k -th HMD adheres to the free-space path loss model, which can be detailed as [11], [12]:

$$\tilde{\mathbf{H}}_n = \mathbf{H} \sqrt{\beta_{0,n} F(\psi_0)}, \quad \forall n \in \mathcal{N}, \quad (4)$$

$$\tilde{\mathbf{g}}_{k,n} = \mathbf{g}_{k,n} \sqrt{\beta_{k,n} F(\psi_k)}, \quad \forall k \in \mathcal{K}, \forall n \in \mathcal{N}, \quad (5)$$

$$\beta_{k',n} = \sqrt{c_0} \|\mathbf{d}_{k',n}\|^{-\frac{\alpha_{k'}}{2}}, \quad k' \in \mathcal{K} \cup \{0\}, \forall n \in \mathcal{N}, \quad (6)$$

where $\beta_{0,n}$ and $\beta_{k,n}$ symbolize the path loss with c_0 being the reference channel power at a distance of 1 meter, while α_0 and $\alpha_k, \forall k \in \mathcal{K}$ are the path loss exponents of AP–IRS and IRS– k -th HMD links, respectively. Moreover, the small-scale fading of the links between AP and IRS, (4), and between IRS and the k -th HMD, (5), are denoted by $\mathbf{H} \in \mathbb{C}^{M \times L}$ and $\mathbf{g}_{k,n} \in \mathbb{C}^{M \times 1}$, respectively. Besides, the distance vectors from the IRS to the AP and k -th HMD, coming from (6), are respectively given by:

$$\mathbf{d}_{0,n} = \mathbf{s}[n] - \mathbf{a} = \\ = [s_x[n] - a_x, s_y[n] - a_y, s_z[n] - a_z]^T, \quad \forall n \in \mathcal{N}, \quad (7)$$

$$\mathbf{d}_{k,n} = \mathbf{s}[n] - \mathbf{u}[n, k] = \\ = [s_x[n] - u_x[n, k], s_y[n] - u_y[n, k], s_z[n] - u_z[n, k]]^T, \quad \forall k \in \mathcal{K}, \forall n \in \mathcal{N}. \quad (8)$$

Therefore, the received signal of k -th HMD follows as:

$$y_{k,n} = \tilde{\mathbf{g}}_{k,n}^H \Theta \tilde{\mathbf{H}} \mathbf{w}_k b_{k,n} + n_k, \quad \forall k \in \mathcal{K}, \forall n \in \mathcal{N}, \quad (9)$$

where $b_{n,k}$ is the bearing-information transmitted symbol for the k -th HMD with normalized power at n -th time slot, $\mathbf{w}_k \in \mathbb{C}^{L \times 1}$ is the transmit beamforming vector, and n_k is the additive white Gaussian noise (AWGN), which follows a complex normal distribution with zero mean and variance σ_k^2 . The IRS phase shifts matrix is represented by Θ and is defined as $\Theta = \text{diag}(\theta_1, \theta_2, \dots, \theta_M) \in \mathbb{C}^{M \times M}$, where $\theta_m = \varrho_m e^{j\vartheta_m} \in \mathbb{C}$ characterizes the reflection coefficient of the m -th IRS element, in which $\varrho_m \in [0, 1]$ is the reflection amplitude¹, and $\vartheta_m \in [0, 2\pi]$ is the phase shifts. Ultimately, by assuming there is no multi-user interference, we represent the SNR at k -th HMD in time slot n as:

$$\gamma_{k,n}(\mathbf{W}, \Theta, \beta, \Psi) = \frac{\beta_{0,n} F(\psi_0) \beta_{k,n} F(\psi_k) |\mathbf{g}_{k,n}^H \Theta \mathbf{H} \mathbf{w}_k|^2}{\sigma_k^2}, \quad \forall k \in \mathcal{K}, \forall n \in \mathcal{N}, \quad (10)$$

where \mathbf{W} , β , and Ψ are the collection of \mathbf{w} 's, β 's and ψ 's according to $\mathbf{W} \triangleq [\mathbf{w}_1, \dots, \mathbf{w}_K]$, $\beta \triangleq [\beta_{0,0}, \dots, \beta_{0,n}, \dots, \beta_{K,N}]$, and $\Psi \triangleq [\psi_0, \dots, \psi_K]$. Consequently, the achievable data-rate of the k -th HMD during the n -th time slot, measured in [bit/s/Hz], can be expressed as:

$$R(\mathbf{W}, \Theta, \beta, \Psi) = \log_2(1 + \gamma_{k,n}(\mathbf{W}, \Theta, \beta, \Psi)), \\ \forall k \in \mathcal{K}, \forall n \in \mathcal{N}. \quad (11)$$

¹To maximize reflection efficiency, we assume the amplitudes of all passive elements to be one [4], [13], i.e., $\varrho_m = 1, \forall m \in \mathcal{M}$.

Finally, the sum data-rate for all HMDs can be written as:

$$R_{\text{tot}}(\mathbf{W}, \Theta, \beta, \Psi) = B \sum_{\forall k \in \mathcal{K}} \sum_{\forall n \in \mathcal{N}} R(\mathbf{W}, \Theta, \beta, \Psi), \quad (12)$$

where B represents the bandwidth of the network.

We aim for system-level data-rate optimization in an IRS-assisted single-cell multi-user indoor VR network. This can be achieved through location-based IRS resource allocation and by adjusting parameters such as transmit beamforming and respective phase shifts and radiation patterns. With these considerations, we can frame the optimization problem as:

$$\max_{\mathbf{W}, \Theta, \beta, \Psi} R_{\text{tot}}(\mathbf{W}, \Theta, \beta, \Psi), \quad (13)$$

$$\text{s.t. } \text{tr}(\mathbf{W} \mathbf{W}^H) \leq P_{\text{AP}}^{\max}, \quad (13a)$$

$$|\theta_m| \leq 1, \quad \forall m \in \mathcal{M}, \quad (13b)$$

$$\mathbf{s}[n] \in \mathcal{H}_q, \quad \forall q \in \{1, \dots, 4\}, \quad (13c)$$

$$\mathbf{u}[n, k] \in \mathcal{U}_k, \quad \forall k \in \mathcal{K}, \quad (13d)$$

$$0 \leq \psi_k \leq \pi/2, \quad \forall k \in \mathcal{K} \cup \{0\}. \quad (13e)$$

Constraint (13a) ensures that the transmission power remains within the upper limits set for the AP. Constraint (13b) specifies the bounds within which the reflection coefficient for every IRS element must operate. Constraint (13c) ensures the IRS is positioned in one of the corner walls of the room. Next, constraint (13e) confines the radiation pattern. Finally, constraint (13d) confirms that each VR user follows a predefined redirected walking path denoted as \mathcal{U}_k [14]. Given the presence of a non-concave objective function and the non-convex nature of constraint (13b), the optimization problem laid out in (13) is distinctly nonconvex [15]. This inherent complexity makes it challenging to derive a straightforward solution for the problem. As a result, AO methods or approximations are needed to address non-convexity effectively.

III. LOCATION OPTIMIZATION AND RESOURCE ALLOCATION OF IRS IN A VR NETWORK

Optimization problem (13) is non-convex due to the highly coupled optimization variables. In general, there is no well-organized method to solve such problems. However, we propose an AO with low computational complexity to achieve a sub-optimal solution, where a new objective function was proposed to avoid the feasibility problem. In the first and second sub-problems, closed-form optimal solutions are obtained for the active beamforming at the AP and passive beamforming at the IRS. In the third one, a global optimization of the IRS' resource allocation is carried out. Finally, the radiation pattern at the IRS is briefly explored in the last sub-problem.

A. Step 1: AP Active (transmitter-side) Beamforming

We first fix Θ , β , and Ψ consider the optimization of active beamforming. Thus, the corresponding optimization problem with a transformed objective function can then be formulated:

$$\max_{\mathbf{w}_k, \mathbf{W}} \sum_{\forall k \in \mathcal{K}} \sum_{\forall n \in \mathcal{N}} A_{n,k}^0 |\mathbf{g}_{k,n}^H \Theta \mathbf{H} \mathbf{w}_k|^2, \quad (14)$$

$$\text{s.t. } (13a).$$

where $A_{n,k}^0 = \frac{\beta_{0,n} F(\psi_0) \beta_{k,n} F(\psi_k)}{\sigma_k^2}$. One can readily prove that the optimization problem (14) is affine, thus convex. Therefore, we can exploit the properties of convex optimization to derive a closed-form global optimal solution. However, the optimal transmit beamforming is known to be the maximum-ratio transmission (MRT) and is given by [16]:

$$\mathbf{w}_k^* = \sqrt{P_{\text{AP}}^{\max}} (\mathbf{g}_{k,n}^H \boldsymbol{\Theta} \mathbf{H})^H / \| \mathbf{g}_{k,n}^H \boldsymbol{\Theta} \mathbf{H} \|, \forall k \in \mathcal{K}. \quad (15)$$

B. Step 2: IRS Passive (receiver-side) Beamforming

Given the optimal active beamforming from the previous sub-problem and fixed β and Ψ , the IRS passive beamforming sub-problem can be recast as:

$$\begin{aligned} \max_{\boldsymbol{\Theta}} \sum_{\forall k \in \mathcal{K}} \sum_{\forall n \in \mathcal{N}} A_{n,k}^0 & | \text{vec}(\boldsymbol{\Theta})^H \boldsymbol{\Upsilon}_n |^2, \\ \text{s.t. } |\theta_m| &= 1, \forall m \in \mathcal{M}, \end{aligned} \quad (16)$$

where we used the change of variables $\mathbf{g}_{k,n}^H \boldsymbol{\Theta} \mathbf{H} \mathbf{w}_k = \text{vec}(\boldsymbol{\Theta})^H \boldsymbol{\Upsilon}_{k,n}$, in which $\boldsymbol{\Upsilon}_n = \text{diag}(\mathbf{g}_{k,n}) \mathbf{H} \mathbf{w}_k$, $\forall n \in \mathcal{N}$. Despite the non-convex nature of the problem (16) due to the unit modulus constraints, a closed-form solution can be derived based on the quadratic transform method. To do so, we rewrite the problem into its equivalent form as:

$$\begin{aligned} \max_{\boldsymbol{\Theta}} \sum_{\forall k \in \mathcal{K}} \sum_{\forall n \in \mathcal{N}} A_{n,k}^0 & \left(- \text{vec}(\boldsymbol{\Theta})^H \mathbf{U} \text{vec}(\boldsymbol{\Theta}) \right. \\ & \left. + 2\Re\{\text{vec}(\boldsymbol{\Theta})^H \boldsymbol{\Upsilon}_n\} \right), \end{aligned} \quad (17)$$

s.t. (16a),

where $\mathbf{U} = \text{vec}(\boldsymbol{\Theta}) \boldsymbol{\Upsilon}_n^H$. Now, we obtain the following simpler upper bound to the quadratic term $\text{vec}(\boldsymbol{\Theta})^H \mathbf{U} \text{vec}(\boldsymbol{\Theta})$:

$$\begin{aligned} \text{vec}(\boldsymbol{\Theta})^H \mathbf{U} \text{vec}(\boldsymbol{\Theta}) & \leq \text{vec}(\boldsymbol{\Theta})^H \mathbf{Q} \text{vec}(\boldsymbol{\Theta}) \\ & - 2\Re\left\{ \text{vec}(\boldsymbol{\Theta})^H (\mathbf{Q} - \mathbf{U}) \text{vec}(\boldsymbol{\Theta}^t)^H \right\} \\ & + \text{vec}(\boldsymbol{\Theta}^t)^H (\mathbf{Q} - \mathbf{U}) \text{vec}(\boldsymbol{\Theta}^t), \end{aligned} \quad (18)$$

where $\mathbf{Q} = \lambda_{\max}(\mathbf{U}) \mathbf{I}_M$ and $\lambda_{\max}(\mathbf{U})$ corresponds to the maximum eigenvalue of the semi-positive definite matrix \mathbf{U} . Additionally, the superscript t indicates the feasible solution achieved during the t -th iteration. Thus, the objective function of (17) can be lower bounded by $-\lambda_{\max}(\mathbf{U}) \|\text{vec}(\boldsymbol{\Theta})\|^2 + 2\Re\{\text{vec}(\boldsymbol{\Theta})^H ((\mathbf{Q} - \mathbf{U}) \text{vec}(\boldsymbol{\Theta}^t) + \boldsymbol{\Upsilon}_n)\} - \text{vec}(\boldsymbol{\Theta}^t)^H (\mathbf{Q} - \mathbf{U}) \text{vec}(\boldsymbol{\Theta}^t)$. Then, we can reformulate the IRS passive beamforming sub-problem in the following manner:

$$\max_{\boldsymbol{\Theta}} \sum_{\forall k \in \mathcal{K}} \sum_{\forall n \in \mathcal{N}} A_{n,k}^0 \Re\{ \text{vec}(\boldsymbol{\Theta})^H \boldsymbol{\Gamma}_n \}, \quad (19)$$

s.t. $|\theta_m| = 1, \forall m \in \mathcal{M}$, (19a)

where $\boldsymbol{\Gamma} = (\mathbf{Q} - \mathbf{U}) \text{vec}(\boldsymbol{\Theta}^t) + \boldsymbol{\Upsilon}_n$. Ultimately, it can be verified that the optimal solution to (19) is expressible in closed-form, as presented:

$$\theta_m = e^{j\arg(\boldsymbol{\Gamma}_m)}, \forall m \in \mathcal{M}. \quad (20)$$

C. Step 3: IRS Placement at Optimal Locations

In this subsection, we formulate the subproblem wherein the IRS's placement is optimized with fixed active beamforming and fixed IRS's phase shifts and radiation pattern, i.e., \mathbf{W} , Ψ , $\boldsymbol{\Theta}$ are known. Therefore, the optimization problem for the IRS's location-based resource allocation can be written as:

$$\begin{aligned} \max_{\mathbf{s}[n]} \sum_{\forall k \in \mathcal{K}} & \frac{c_0^2 F(\psi_0) F(\psi_k) \left| \mathbf{g}_{k,n}^H \boldsymbol{\Theta} \mathbf{H} \mathbf{w}_k \right|^2}{\sigma_k^2 \|\mathbf{s}[n] - \mathbf{a}\|^{\alpha_0} \|\mathbf{s}[n] - \mathbf{u}[n, k]\|^{\alpha_k}}, \\ \text{s.t. (13c) and (13d),} \end{aligned} \quad (21)$$

where β 's are replaced by the IRSs' location decision variables, $\mathbf{s}[n]$. It can be seen that (21) is convex. Thus, an optimal solution for the IRSs' placement can be found. Assuming $\alpha_k = 2$ [17] and by setting the first-order derivative of the objective function with respect to $\mathbf{s}[n]$ to zero, we obtain the following equalities:

$$\begin{aligned} & \frac{(a_x - s_x[n])}{(a_x - s_x[n])^2 + (a_y - s_y[n])^2 + (a_z - s_z[n])^2} \\ & = \frac{(s_x[n] - u_y[n, k])}{(s_x[n] - u_y[n, k])^2 + (s_y[n] - u_y[n, k])^2 + (s_z[n] - u_z[n, k])^2}, \end{aligned} \quad (22)$$

$$\begin{aligned} & \frac{(a_y - s_y[n])}{(a_x - s_x[n])^2 + (a_y - s_y[n])^2 + (a_z - s_z[n])^2} \\ & = \frac{(s_y[n] - u_y[n, k])}{(s_x[n] - u_y[n, k])^2 + (s_y[n] - u_y[n, k])^2 + (s_z[n] - u_z[n, k])^2}, \end{aligned} \quad (23)$$

$$\begin{aligned} & \frac{(a_z - s_z[n])}{(a_x - s_x[n])^2 + (a_y - s_y[n])^2 + (a_z - s_z[n])^2} \\ & = \frac{(s_z[n] - u_z[n, k])}{(s_x[n] - u_y[n, k])^2 + (s_y[n] - u_y[n, k])^2 + (s_z[n] - u_z[n, k])^2}, \end{aligned} \quad (24)$$

where an iterative approach could be employed to determine the optimal locations for IRS. With the knowledge of the AP location and the HMDs' trajectory [18], we initialize with predefined values for $s_x[n]$, $s_y[n]$, and $s_z[n]$. From these, we deduce the optimal IRS coordinates iteratively, based on equations (23) – (25), while simultaneously satisfying the constraint (13c) and (13d).

D. Step 4: IRS Radiation Pattern Optimization

We now consider the last subproblem of optimizing Ψ with fixed \mathbf{W} , $\boldsymbol{\Theta}$, and β , which can be given by:

$$\begin{aligned} \max_{\Psi} \sum_{\forall k \in \mathcal{K}} \sum_{\forall n \in \mathcal{N}} & A_{n,k}^1 \cos^3(\psi_0) \cos^3(\psi_k), \\ \text{s.t. (13e),} \end{aligned} \quad (25)$$

where $A_{n,k}^1 = \frac{\beta_{0,n} \beta_{k,n} \left| \mathbf{g}_{k,n}^H \boldsymbol{\Theta} \mathbf{H} \mathbf{w}_k \right|^2}{\sigma_k^2}$. Unlike the preceding subproblems, where we had to work out how to get to the closed-form solutions algebraically, obtaining a closed-form solution is straightforward due primarily to the monotonicity of cosine terms in the objective function. Fortunately, it can be readily proved the endpoints of the interval in (13e) yield the global

Algorithm 1 Iterative AO algorithm

Input: Set $i = 0$, I_{\max} , and initialize $\mathbf{W} = \mathbf{W}^0$, $\Theta = \Theta^0$, $\beta = \beta^0$, and $\Psi = \Psi^0$.

- 1: **Repeat**
- 2: Solve problem (14) for given $\{\Theta^{i-1}, \beta^{i-1}, \Psi^{i-1}\}$ and use (15) to obtain the optimal solution \mathbf{W}^i .
- 3: Solve problem (19) for given $\{\mathbf{W}^{i-1}, \beta^{i-1}, \Psi^{i-1}\}$ and use (20) to obtain the optimal solution Θ^i .
- 4: Solve problem (21) for given $\{\mathbf{W}^{i-1}, \Theta^{i-1}, \Psi^{i-1}\}$ and use (23)–(25) to obtain the optimal solution β^i .
- 5: Solve problem (25) for given $\{\mathbf{W}^{i-1}, \Theta^{i-1}, \beta^{i-1}\}$ to obtain the optimal solution Ψ^i .
- 6: **until** $i = I_{\max}$
- 7: **Return** $\{\mathbf{W}^*, \Theta^*, \beta^*, \Psi^*\} = \{\mathbf{W}^i, \Theta^i, \beta^i, \Psi^i\}$.

maximum of the objective function as $\cos^3(\psi_k), \forall k \in \mathcal{K} \cup \{0\}$ is monotonically decreasing when $0 \leq \psi_k \leq \pi/2$. This implies that an elevation angle of zero results in the most favorable IRS radiation patterns. The final iterative-based AO approach is provided in **Algorithm 1**.

IV. COMPLEXITY ANALYSIS

In this section, we conduct an analysis of the computational complexity of our proposed algorithm. The AO algorithm iteratively tackles the four subproblems related to \mathbf{W} , Θ , β , and Ψ until convergence is reached. We obtain efficient closed-form solutions for the first two subproblems, as in (15) and (20), respectively. The last two subproblems have been convexified and can be efficiently solved in polynomial time using CVX [4]. The computational complexities associated with \mathbf{W} , Θ , β , and Ψ are as follows: $O_1 = \mathcal{O}(KL^3)$, $O_2 = \mathcal{O}(K^2LNM + K^2M^2 + M^3)$, $O_3 = \mathcal{O}((3N)(12N + 3NK)^3)$, and $O_4 = \mathcal{O}((K+1)^3)$. Hence, the proposed AO algorithm's computational complexity can be approximated as $\mathcal{O}(KL^3 + K^2LNM + K^2M^2 + M^3 + N^4K^3)$.

V. EVALUATION SETUP AND RESULTS

We utilize a simulation framework for assessing the performance of the AO algorithm in an IRS-assisted full-immersive Virtual Reality (VR)-supporting mmWave network, accounting for the locations of the HMD VR users, the AP, and the IRS within a 3D environment. The allocation of IRS resources is considered within the environment's four outer walls, excluding floor and ceiling. The AP is centered on the ceiling at 3 m height with the HMDs navigating in environments sized 10×10 , 15×15 , or 20×20 m^2 [18].

The proposed AO algorithm is derived for a generic number of IRS elements, where the allocation of the number of such resources will depend on the communication data-rate requirements of the future VR systems. Initially, we consider 200 such elements, each sized $\lambda/5$ [19], [20]. We utilize the discrete-event network simulator (ns-3), in particular its WiGig module, which facilitates the analysis of the IEEE

TABLE I: Overview of baseline simulation parameters.

Parameter Name	Parameter Value
Application Type	OnOffApplication
Data Rate	150 Mbps
Flow Direction	Downlink
Payload Size	1448 Bytes
Transport Protocol	UDP
MAC Queue Size	4000 Packets
Aggregation Type	A-MSDU and A-MPDU
MAC / PHY	CSMA/CA / SC DMG MCS-10
Transmit Power / Sectors	10 mW / 8
Rx Noise Figure	10 dB
Operating Frequency	60.48 GHz

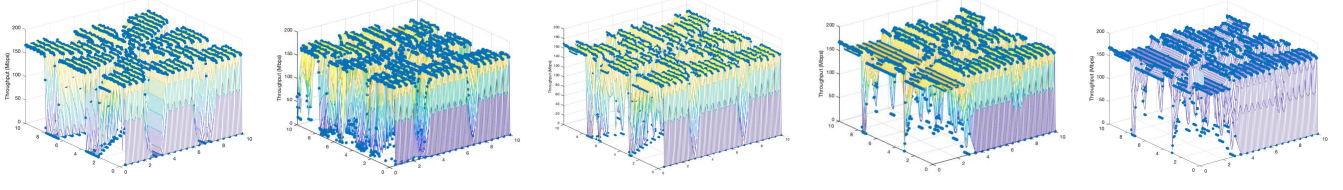
TABLE II: Summary of achieved results. Different approaches are compared based on room sizes, their average (Avg) throughput, and standard deviation (SD).

Approach	Room size [m^2]	Avg [Mbps]	SD [Mbps]
No IRS	10×10	124, 08	68, 4051
	15×15	112, 25	74, 7407
	20×20	98, 063	79, 2939
Random	10×10	131, 97	60, 4667
	15×15	117, 58	62, 8617
	20×20	109, 40	67, 1633
Optimal	10×10	144, 97	50, 5537
	15×15	125, 10	68, 5524
	20×20	115, 87	72, 2035
Oracle	10×10	147, 89	40, 4191
	15×15	129, 34	47, 5146
	20×20	118, 74	49, 0862
Best Path	10×10	148, 90	39, 1131
	15×15	131, 34	46, 5221
	20×20	120, 73	48, 9770

802.11ad/ay protocols' performance [21]. Moreover, we incorporate a mmWave propagation model into the existing ns-3 framework that models the presence of the IRS on signal propagation in the environment [11], [12]. The summary of relevant simulation parameters is given in TABLE I.

The “Optimal” approach follows Algorithm 1 for dynamically adjusting the IRS configuration and resources allocation based on the HMD, AP, and IRS locations, and IRS radiation patterns. We further consider the IRS's placement at a “Random” location, as well as at an “Oracle” location that identifies the IRS's placement in all potential locations across room walls with 0.1m-sized grid, and does that for every HMD location. Besides, the “Best path” is used to assess the performance of the combination of the direct AP-HMD and AP-IRS-HMD links, with the IRS's placement utilizing the “Optimal” approach.

We evaluate the performance of different approaches and express it through average throughput and its standard deviation (SD) against a maximum threshold of 150 Mbps per HMD, focusing on scenarios with a single and multiple HMDs navigating through different environments (cf., TABLE II). A snapshot of the results, focusing on the $10 \times 10 m^2$ environment, is depicted in Figure 2. The throughput in each environment peaks when the IRS is optimally positioned for each HMD, in comparison to scenarios without an IRS and with its resource allocation at a random location. The IRS resource allocation at an oracle location occasionally results in a higher throughput,



(a) No IRS (b) IRS at a random location (c) IRS at an optimal location (d) IRS at an oracle location (e) LoS + IRS at optimal

Fig. 2: Communication coverage achieved by different approaches in a $10 \times 10 \text{ m}^2$ room.

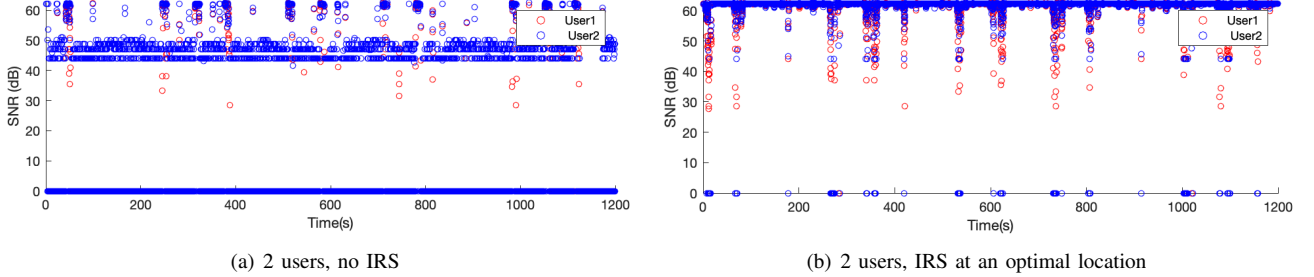


Fig. 3: SNR variability enhancements due to the utilization of IRS resources at locations optimized by the proposed AO approach.

yet the AO algorithm can closely match its performance for the majority of HMD locations despite its real-time-operating nature. Notably, the average throughput considering both the optimal IRS path and direct HMD-AP channel is highly comparable to the oracle. Analyzing SD, the performance of the network without an IRS shows higher throughput variability across environments compared to the scenarios with IRS support, even for its random resource allocation in the environment. Moreover, the “Optimal” location-based IRS resource allocation yielded by the AO approach, as well as its combination with Line-of-Sight (LoS) communication, offer consistent throughput and low SNR variability, even in multi-user scenarios (cf., Figure 3).

VI. CONCLUSION

We have proposed an Alternating Optimization (AO) algorithm that determines the allocation of Intelligent Reflective Surface (IRS) resources based on the relative locations of the Head Mounted Devices (HMDs) and Access Point (AP) in full-immersive multiuser Virtual Reality (VR)-supporting millimeter Wave (mmWave) networks. Our algorithm paves a new avenue for enhancing the immersiveness of VR by integrating IRSs into the supporting high data-rate wireless communication network. Our evaluation results underscore the potency of the proposed algorithm and the potential of IRSs in enhancing communication coverage and improving users’ Virtual Experiences (VEs).

REFERENCES

- [1] L. Muñoz-Saavedra *et al.*, “Augmented and virtual reality evolution and future tendency,” *Applied sciences*, vol. 10, no. 1, p. 322, 2020.
- [2] M. Chen *et al.*, “Virtual reality over wireless networks: Quality-of-service model and learning-based resource management,” *IEEE Trans. Commun.*, vol. 66, no. 11, pp. 5621–5635, 2018.
- [3] J. Jalali *et al.*, “Is active IRS useful for mmwave wireless networks or not?,” in *Proc. IEEE Int. Conf. Computing, Netw. Commun. (ICNC)*, pp. 377–382, 2023.
- [4] J. Jalali *et al.*, “IRS-based energy efficiency and admission control maximization for iot users with short packet lengths,” *IEEE Trans. Veh. Technol.*, vol. 72, no. 9, pp. 12379–12384, 2023.
- [5] F. Lemic *et al.*, “Localization in power-constrained terahertz-operating software-defined metamaterials,” *ELSEVIER Nano Commun. Netw.*, vol. 30, p. 100365, 2021.
- [6] C. Chaccour *et al.*, “Risk-based optimization of virtual reality over Terahertz reconfigurable intelligent surfaces,” in *Proc. IEEE Int. Conf. Commun. (ICC)*, pp. 1–6, 2020.
- [7] K.-L. Besser *et al.*, “Reconfigurable intelligent surface phase hopping for ultra-reliable communications,” *IEEE Trans. Wirel. Commun.*, vol. 21, no. 11, pp. 9082–9095, 2022.
- [8] Y. Zhou *et al.*, “Latency minimization for secure intelligent reflecting surface enhanced virtual reality delivery systems,” *IEEE Wirel. Commun. Lett.*, vol. 11, no. 9, pp. 1770–1774, 2022.
- [9] E. R. Bachmann *et al.*, “Multi-user redirected walking and resetting using artificial potential fields,” *IEEE Trans. Vis. Comput. Graph.*, vol. 25, no. 5, pp. 2022–2031, 2019.
- [10] W. Tang *et al.*, “Wireless communications with reconfigurable intelligent surface: Path loss modeling and experimental measurement,” *IEEE Trans. Wirel. Commun.*, vol. 20, no. 1, pp. 421–439, 2021.
- [11] E. Björnson *et al.*, “Power scaling laws and near-field behaviors of massive MIMO and intelligent reflecting surfaces,” *IEEE Open J. Commun. Soc.*, vol. 1, pp. 1306–1324, 2020.
- [12] J. Jalali *et al.*, “Power-efficient joint resource allocation and decoding error probability for multiuser downlink MISO with finite block length codes,” in *Proc. IEEE Wirel. Personal Multimed. Commun. (WPMC)*, pp. 232–237, 2022.
- [13] J. Jalali *et al.*, “Toward energy efficient multiuser IRS-assisted URLLC systems: A novel rank relaxation method,” in *Proc. IEEE Glob. Commun. Conf. Wkshps. (Globecom Wkshps.)*, pp. 1–7, 2023.
- [14] F. Lemic *et al.*, “Predictive context-awareness for full-immersive multiuser virtual reality with redirected walking,” *IEEE Commun. Mag.*, vol. 61, no. 9, pp. 32–38, 2023.
- [15] J. Jalali *et al.*, “Power-efficient antenna switching and beamforming design for multi-user SWIPT with non-linear energy harvesting,” in *2023 Proc. IEEE Consumer Commun. Netw. Conf. (CCNC)*, pp. 746–751, 2023.
- [16] J. Jalali *et al.*, “Joint offloading policy and resource allocation in IRS-aided MEC for IoT users with short packet transmission,” in *Proc. IEEE Veh. Technol. Conf. (VTC2023-Fall)*, pp. 1–7, 2023.
- [17] J. Jalali *et al.*, “Optimal resource allocation for MC-NOMA in swipt-enabled networks,” *IEEE Comm. Letters*, pp. 2250–2254, 2020.
- [18] T. Van Onsem *et al.*, “Toward full-immersive multiuser virtual reality with redirected walking,” *IEEE Access*, pp. 24722–24736, 2023.
- [19] K.Ntontin *et al.*, “optimal reconfigurable intelligent surface placement in millimeter-wave communications,” in *EuConf.AntennPropag*, pp.1–5, 2021
- [20] Ö. Özdogan *et al.*, “Intelligent reflecting surfaces: Physics, propagation, and pathloss modeling,” *IEEE Wirel. Commun. Lett.*, vol. 9, no. 5, pp. 581–585, 2019.
- [21] V. Angelov *et al.*, “Modern virtual reality headsets,” in *Proc. IEEE Hum-Comput Interaction, Optim. Robot. Appl.*, pp. 1–5, 2020.